# Supporting Information for

## Evolution of Eastern Equatorial Pacific Seasonal and Interannual Variability in response to orbital forcing during the Holocene and Eemian from Model Simulations

V.C. Khon[1,2,3]*, B. Schneider[1], M. Latif[3,4], W. Park[3], C. Wengel[3]

Contents of this file

1. Figures S1 to S8

[1]Institute of Geosciences at Kiel University, Kiel, Germany

[2]A.M. Obukhov Institute of Atmospheric Physics, Russian Academy of Sciences, Moscow, Russia

[3]GEOMAR Helmholtz Centre for Ocean Research Kiel, Kiel, Germany

[4]University of Kiel, Kiel, Germany

Geophysical Research Letters, 2018

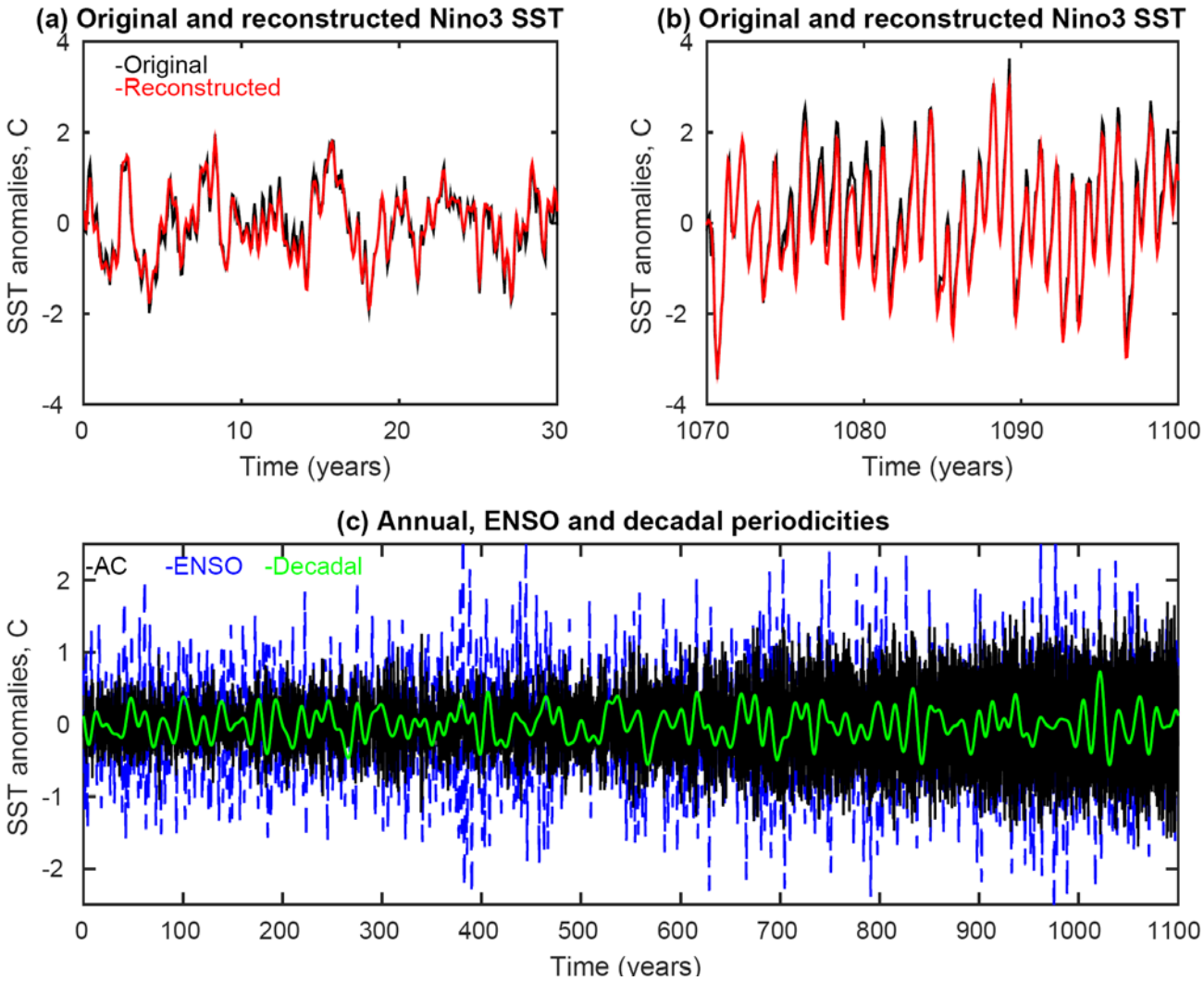


**Figure S1. (c)** Example decomposition of monthly mean Niño3 SST time-series into the annual, interannual and multi-decadal harmonics using the inverse wavelet transform. Transient Eemian simulation is shown where time axis is directed from the early to the late Eemian; **(a,b)** Original and reconstructed time series for the early and late Eemian.

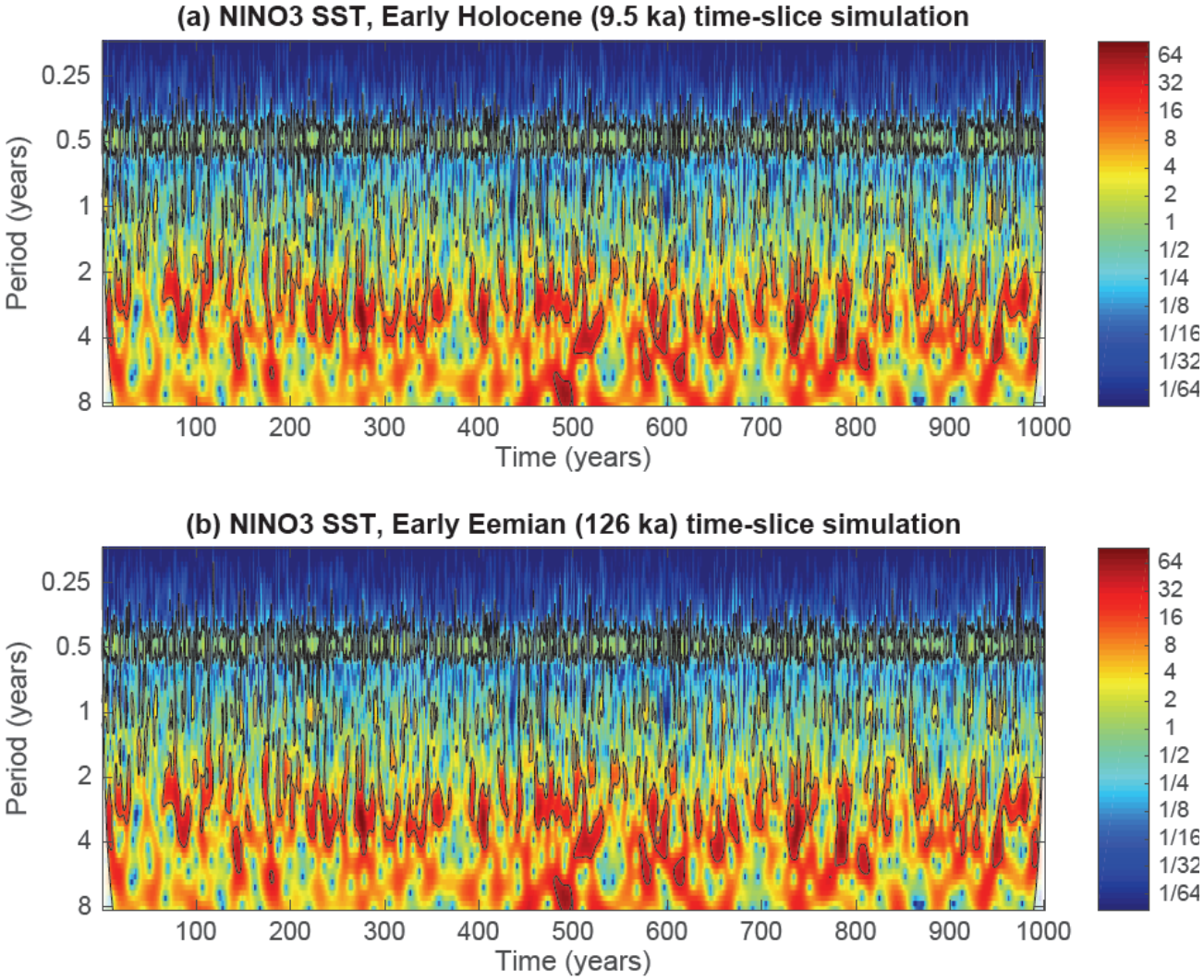


**Figure S2.** Wavelet analysis of monthly mean Niño3 SST from KCM simulations forced by fixed orbital configurations corresponding to the early Holocene (a) and early Eemian (b). Black contours indicate 95% significance levels.

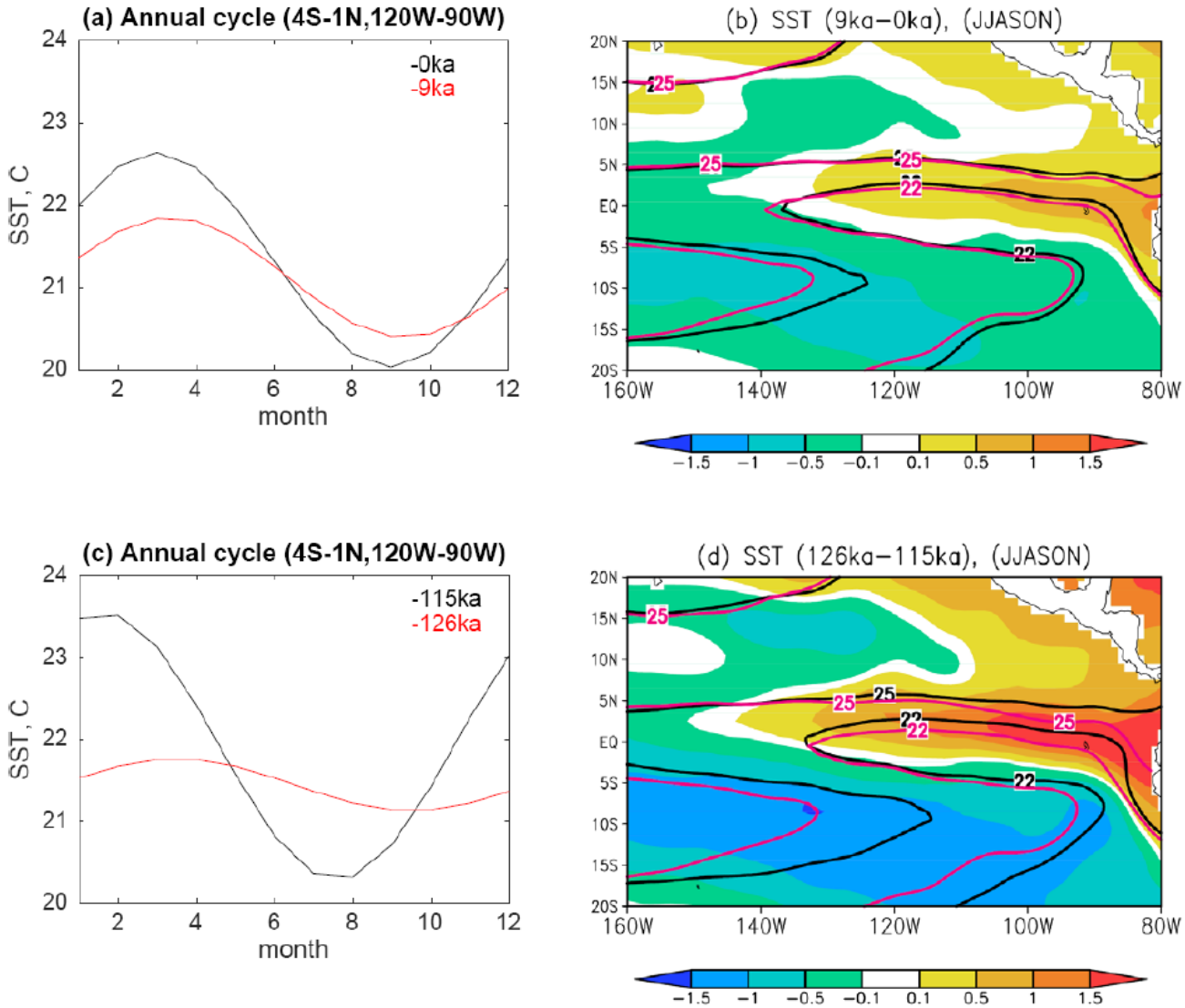


**Figure S3.** (a, c) Annual cycle of SST averaged over the Pacific cold tongue area (4S-1N, 120W-90W) for the Holocene (a) and Eemian (c). (b, d) Mean climatological SST for the early (red contours) and late (black contours) interglacials. Changes in SST (shaded, K) for the cold tongue development season (June to November) between: (b) the early Holocene and preindustrial, (d) the early and late Eemian.

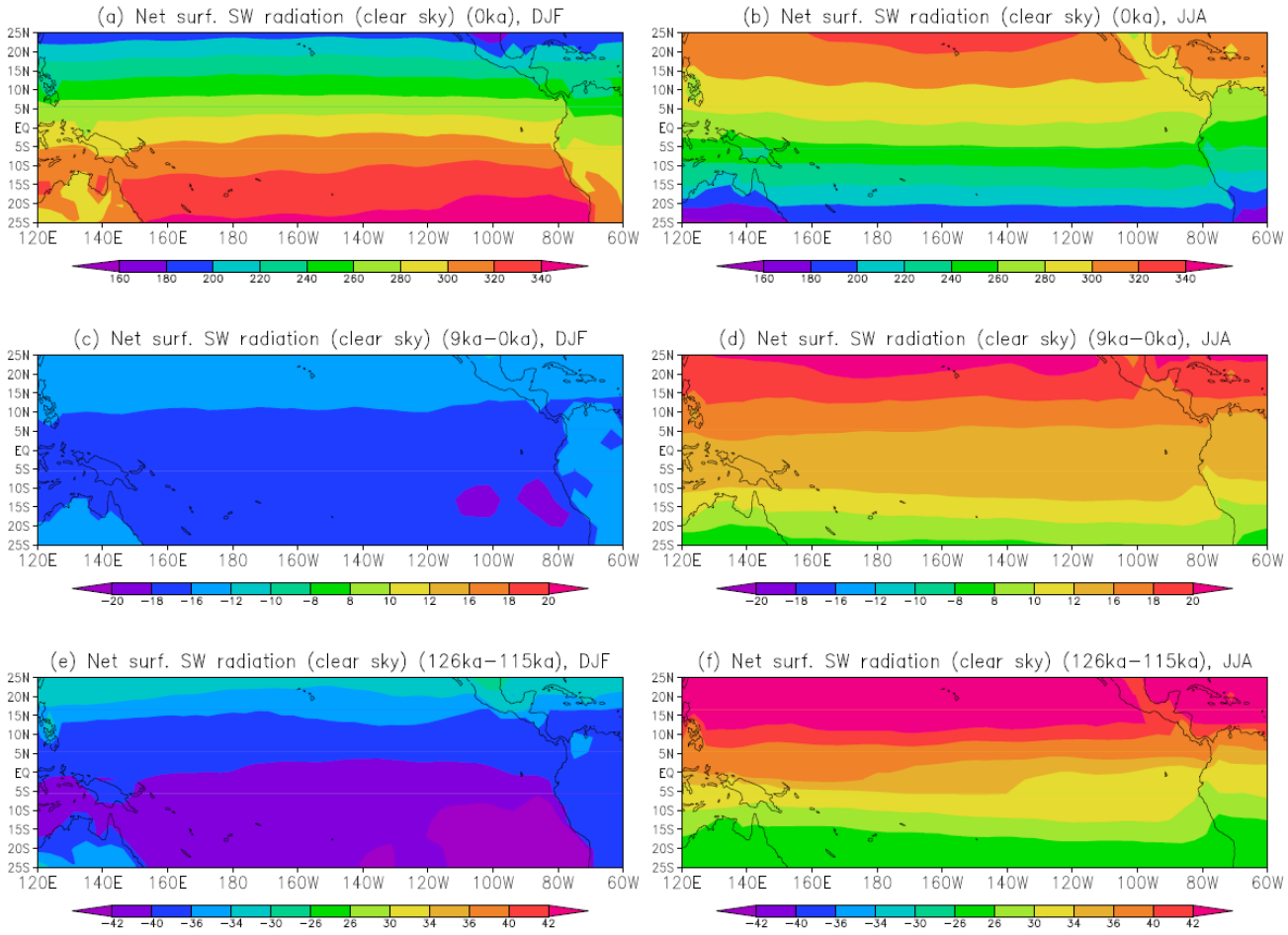


**Figure S4.** Simulated climatological mean net surface shortwave radiation (clear sky, $Wm^{-2}$) for preindustrial (a, b) and its changes between the early Holocene and preindustrial (c, d) and the early and late Eemian (e, f) during boreal winter (a, c) and summer (b, d).

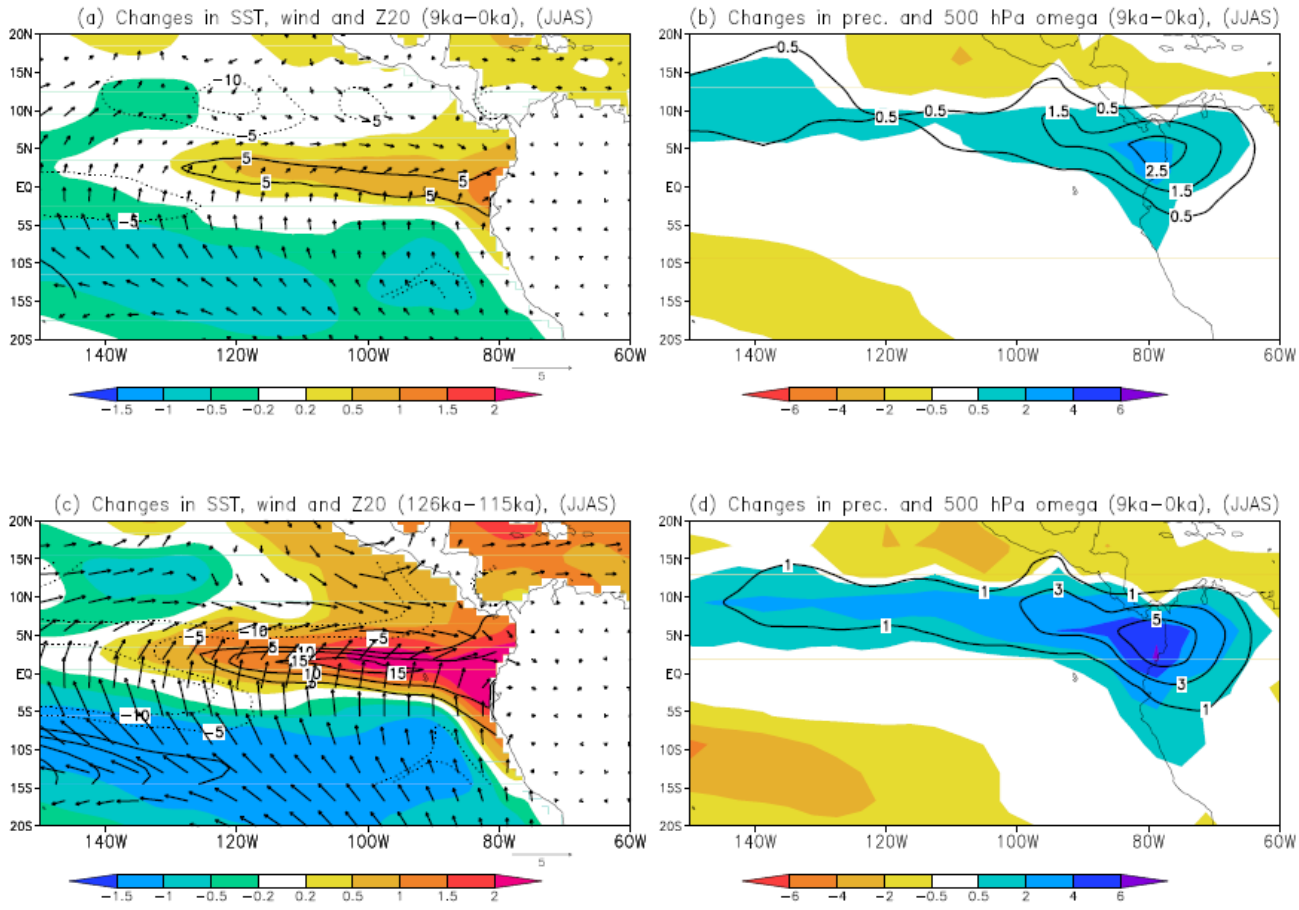


**Figure S5.** (a, b) Changes in SST (shaded, K), surface wind (arrows, m $s^{-1}$) and thermocline depth (m) as defined by 20° C isotherm depth (contours) between the early Holocene and preindustrial (a) and the early and late Eemian (b) for cold season (June to September). (c, d) Changes in precipitation (shaded, mm $day^{-1}$) and vertical velocity at 500 hPa (contours, $10^{-2}$ Pa $s^{-1}$) between the early Holocene and preindustrial (c) and the early and late Eemian (d).

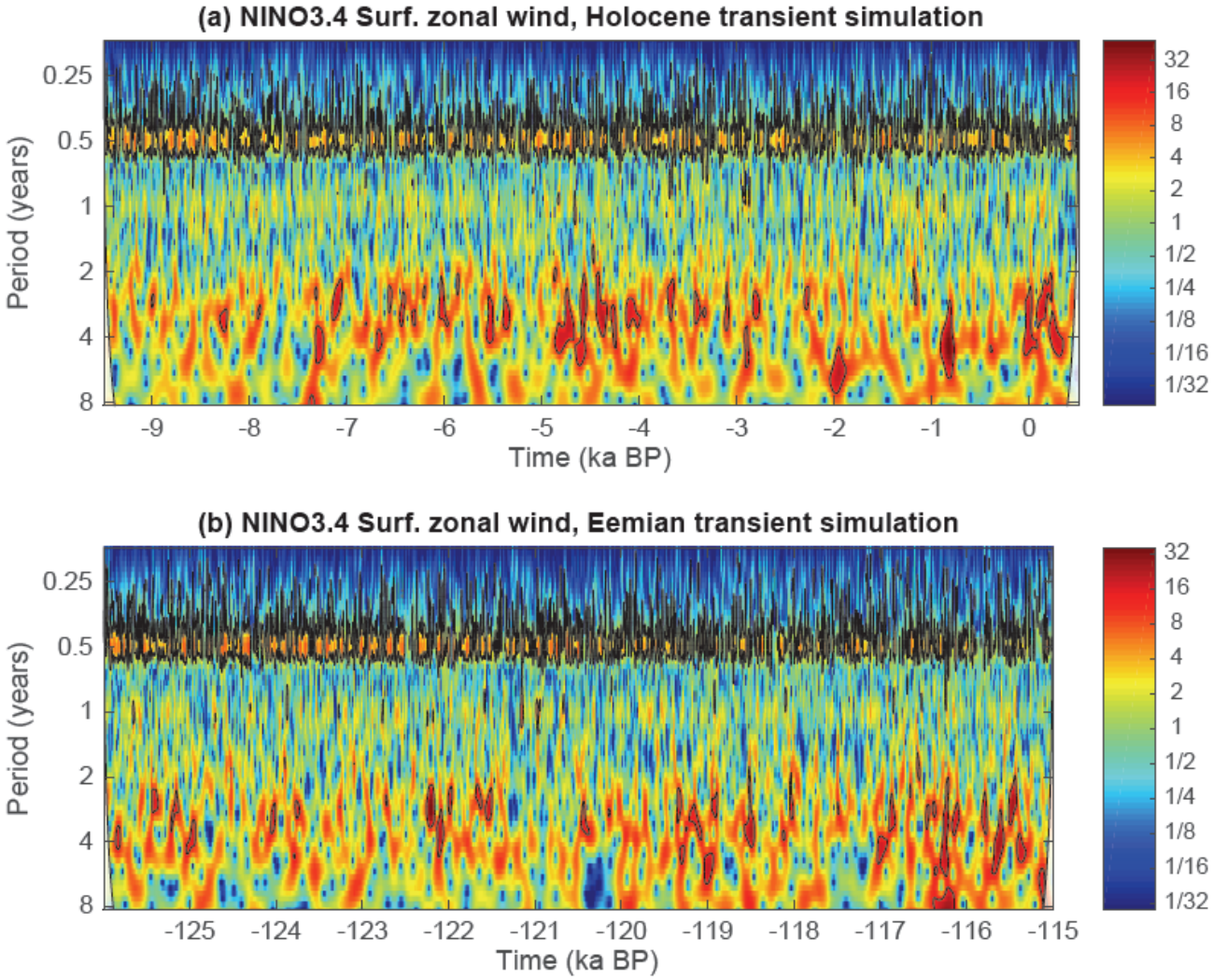


**Figure S6.** Wavelet analysis of monthly-mean surface zonal wind averaged over Niño3.4 region (5°S-5°N, 170°W-120°W) simulated by the KCM for the Holocene (a) and Eemian (b). Black contours indicate 95% significance levels.

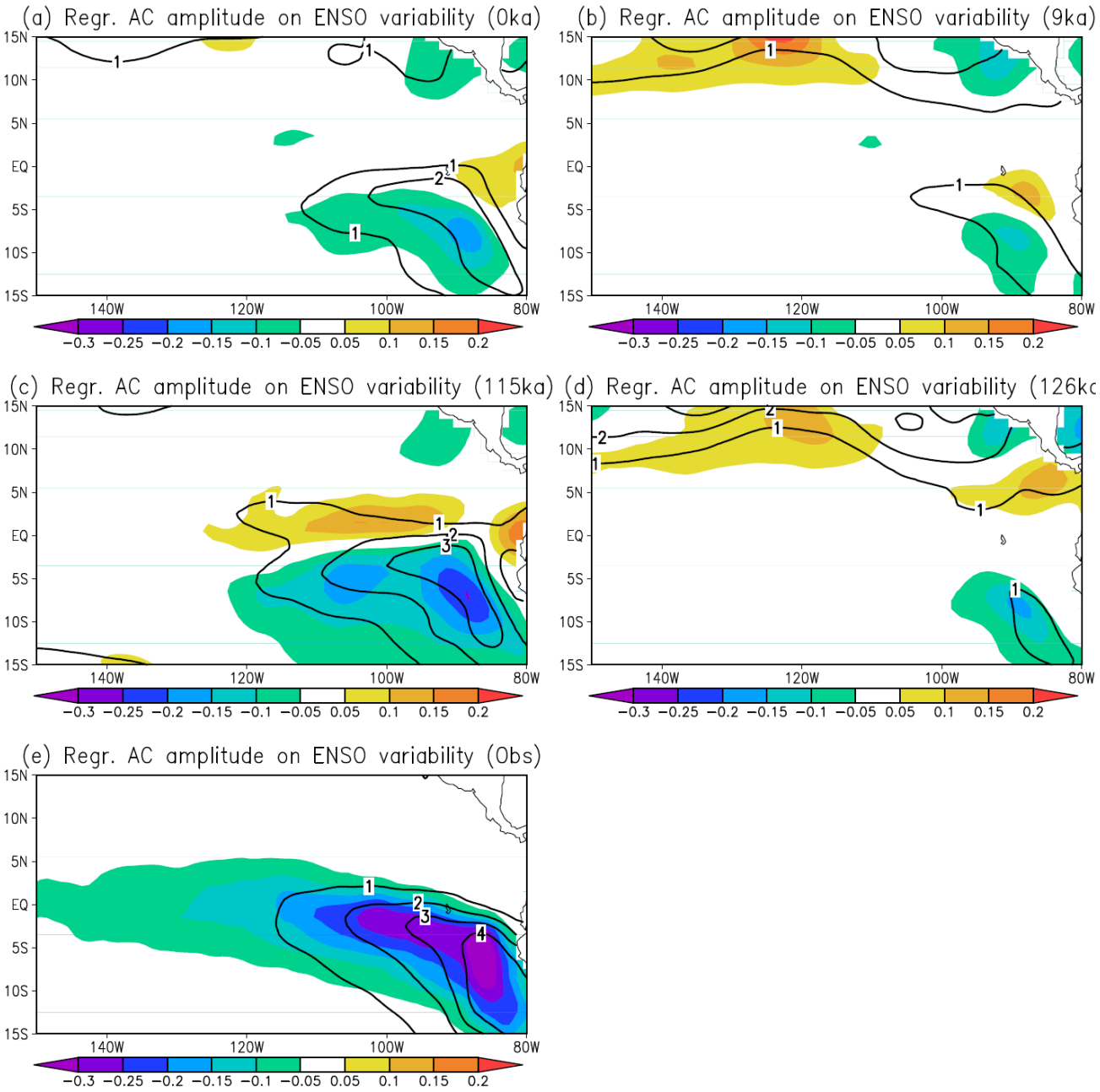


**Figure S7.** Regression (K/K) of amplitude of the SST annual cycle (AC amplitude) on interannual variability of Niño3 SST (ENSO, shaded) as observed (e) and simulated by the KCM for the Holocene (a,b) and Eemian (c,d). Countors show mean AC amplitudes (K). The regression is calculated as Cov(ENSO, AC amplitude)/Var(ENSO).

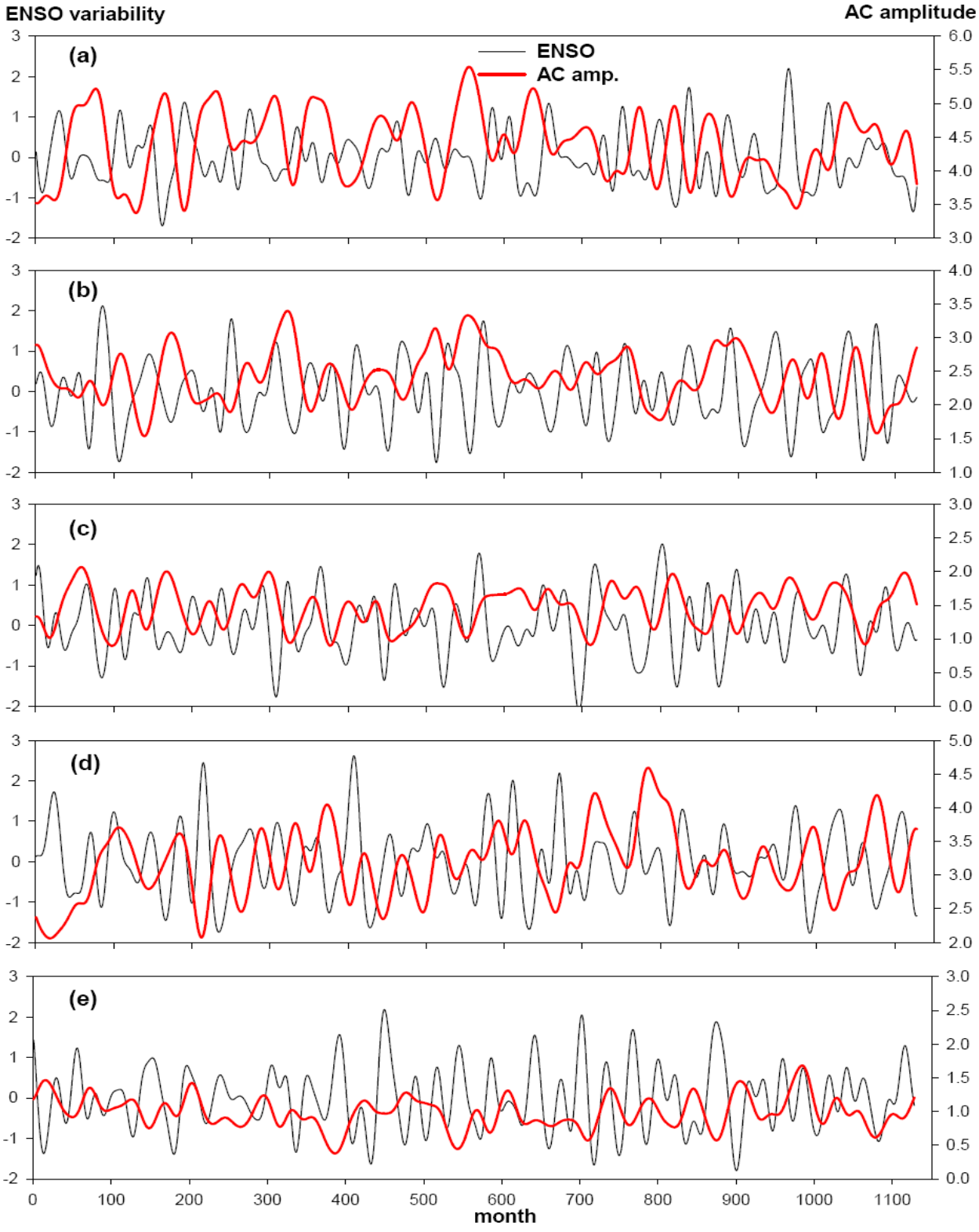


**Figure S8.** Time series of interannual variability (ENSO) and amplitude of annual cycle (AC) of SST averaged over the southeastern tropical Pacific region (10°S-5°S, 90°W-85°W) according to observations (a) and KCM simulations for preindustrial (b), 9 ka (c), 115 ka (d) and 126 ka (e) BP.